Simulation of the electron cloud in the Fermilab Main Injector

FERMILAB-PUB-11-228-APC-CD

Paul L. G. Lebrun,[1] Seth A. Veitzer,[2] Peter Stoltz,[2]

Panagiotis G. Spentzouris,[1] and John R. Cary[2]

[1] *Fermi National Accelerator Laboratory*[*]

[2] *Tech-X, Boulder, Colorado, USA*

(Dated: May 26, 2011)

Abstract

We present results from a precision simulation of the electron cloud (EC) problem in the Fermilab Main Injector using the code VORPAL. This is a fully 3d and self consistent treatment of the EC. Both distributions of electrons in 6D phase-space and EM field maps have been generated. Various configurations of the magnetic fields found around the machine have been studied. Plasma waves associated to the fluctuation density of the cloud have been analyzed. Our results have been successfully benchmarked against the POSINST code for the 2D electrostatic case. The response of a Retarding Field Analyzer (RFA) to the EC has been simulated as well as the more challenging microwave absorption experiment. While numerically accurate predictions can be made for a given secondary emission yield (SEY) and initial conditions, the large uncertainties in this SEY and in the spatial distribution of the EC prior to the exponential growth of the EC do make *ab-initio* prediction difficult. Note also that the RFA response is also uncertain due to the collection efficiency in unknown stray magnetic fields. Nonetheless, our simulations do provide guidance to the experimental program. Moreover, for a reasonable set of initial condition, this calculation shows that no dramatic, non-linear, increase of the EC density will occur when the bunch charges increases by a factor of three. Finally, electric field maps or parametric functions are being provided to the Synergia tracking code such that instabilities due to the EC can be simulated over much longer periods of time.

PACS numbers: 29.27.-a

[*] lebrun@fnal.gov

Operated by Fermi Research Alliance, LLC under Contract No. DE-AC02-07CH11359 with the United States Department of Energy

I. MOTIVATION

The electron cloud (EC) phenomena in high intensity proton storage rings and synchrotrons can limit the performance of such machines [1], [2]. This phenomena is characterized by an exponential growth of the number of low energy (eV) electrons emitted at the surface of the beam pipe wall. Such electrons are then accelerated by the field induced by the passage of the proton beam, which itself causes more secondary emission of electrons at the beam pipe wall. This is reminiscent to the multipacting phenomena observed in R.F. cavities, where one field emission region is replaced the proton beam itself. Such EC can generate fast beam instabilities, as they strongly perturb the electric field in the vicinity of the proton beam. This has been predicted by many models, observed in many e^+e^- storage rings, and studied in detail at CesrTA [3]. The Fermilab Main Injector (MI) is no exception. In the "Project X"[4] era, the delivered beam power on target will go from the current value of 300 MW to 2.1 GW. In a first upgrade, the MI cycle time will be reduced to 1.33 seconds from its current value of 2.2 seconds, thereby increasing the 120 GeV beam power to 700 kW. The second upgrade will require a new injector as the bunch charge will increase by a factor of three. While the MI currently delivers the designed beam intensity, we are concerned that a significant increase of the bunch charge will trigger the formation of a much denser EC, and significantly increase beam losses due to fast instabilities that are hard to control.

Therefore, an R&D initiative has started aiming at providing a robust mitigation strategy. Unlike some e^+e^- storage rings (e.g. KEKB), the MI has relatively short straight sections compared to the length of the arcs, which almost entirely consist of dipoles and quadrupole. Thus, an EC solution based on the use of solenoidal fields that confine the EC away from the beam is simply not applicable. A well established solution would consist in coating the beam pipe with a thin layer of either TiN or amorphous carbon [5], but such a solution could be expensive. Thus, despite the success of numerous previous effort in describing the EC, further R&D on the EC in the MI is well justified, because both the phenomenology and the mitigation strategy have always been site specific.

Furthermore, we present here detailed results on the EC morphology and related fields. This is accomplished using VORPAL [6]. This is a code used for accurate simulation of plasma and beams problems where complicated collective effects are important. Unlike

POSINST [2, 7] and QuickPic [8], two distinct codes originally written to simulate "positron beam instabilities" and used extensively to simulate the response of the beam to the perturbation due to EC, VORPAL is a fully consistent, 3D electromagnetic code using relativistic electrons. Results on a specific benchmark POSINST vs VORPAL will be briefly discussed. While VORPAL allows us to obtain a more precise description of the EC, this can only be done for relatively short sections (2 to 16 m.) of the machine, due to computational limitations. Over such short distances and for relatively short periods of time compared to a full synchrotron cycle, ($\approx 1.0\,\mu$ sec), the electromagnetic fields induced by the EC are not strong enough to perturb the trajectories of the ≈ 20 GeV proton beam. Therefore, the proton beam is assumed to be perfectly rigid, i.e., no changes to its associated current occur throughout the simulation. Obviously, this is not true over long distances and many turns. However, our simulation produces field maps that can be incorporated into the Synergia framework [30] where numerous collective effects can be studied. This will allow us to study the impact of the EC on the beam itself.

Finally, new detectors have been developed in the recent past to characterize the EC. In this paper, we report on both the simulation of the EC phenomena and two distinct instruments: the Retarding Field Analyzer (RFA) [10] and the measurement of phase shifts in microwaves propagating in the MI beam pipe [11].

II. CONFIGURATIONS

A. The Fermilab Main Injector

The Fermilab Main Injector (MI) is a strong focusing high energy synchrotron. A complete description of it is evidently beyond the scope of this paper, but can be found in our Fermilab operating manuals[12, 13]. The relevant features of the MI are summarized on table I. Note that one essential parameter, the Secondary Emission Yield (SEY) at the beam pipe wall, is poorly known. While the SEY can be determined on the bench, it is known to be affected by the complicated surface chemistry in presence of residual gas and irradiation due to beam losses, and the electron cloud itself [14, 15].

We limit our study to the exponential-like growth of the EC due to the interaction of the EC with proton beam and the beam pipe walls, skipping over the details of the generation

of the seed electrons. Suffice to say that electrons are present in the beam pipe at the beginning of a batch, either due to beam losses or gas ionization. Regarding the later mechanism, assuming an ionization production of ≈ 28 ions/cm at STP (assuming a typical Hydrogen, water, Nitrogen, CO mixture) [16, 17], per minimum ionizing protons, the seed density due to gas ionization is estimated to be $1.2\,10^6\,e/m^3$. This density is indeed a very small fraction of the density of high energy protons in the bunch, and as easily shown in previous study does not cause beam instabilities. This seed density is also much smaller than the density reached when multipacting between the beam and beam pipe wall occurs.

Other sources for seed electrons, such as those due to beam losses, are harder to determine. Thus, this implies that our simulation will not give any ab-initio estimate for the timing of the onset of the disturbing EC.

Regarding the transverse emittance, most of the calculations have been done for the worst case scenario for EC, where the emittance are assumed to be small at the onset, thereby inducing transverse electric fields that are sufficiently strong to accelerate the electrons.

B. Modeling of the relevant section of the machine.

A simulation of the EC throughout the full 3.2 km ring is both unnecessary and unrealistic, as it would require too much compute power. The following setups have been implemented in our simulation:

- Short sections with the large radius beam pipe and with small stray magnetic fields. Such straight sections contain one meter coated beam pipe that have been instrumented with RFA's.
- Short (0.25 to 1 m. long) sections of a MI dipole, with uniform dipole fields and an elliptical beam pipe.
- Long ($\sim$ 16 m.) sections of the elliptical beam pipe with a uniform magnetic field. The length is determined by the distance between the antennas used in the microwave experiment. While such a perfectly uniform magnetic field is not realistic, it is has been implemented in the simulation for simplicity and benchmarking purposes.
- Long ($\sim$ 16 m.) sections of the elliptical beam pipe with a MI dipole followed by a MI quadrupole, then a dipole. Realistic fringe fields have been implemented.

TABLE I. Current MI machine and beam parameters.

Parameter	**Value**
Dipole lengths	6.096 m and 4.064 m
Magnetic Field in dipole (20 GeV)	0.234 Tesla
Number of dipoles	216 and 128
Quadrupole Lengths	2.134, 2.539, and 2.945 m
Quadrupole gradient (20 GeV)	2.25 T/m
Number of quadrupole	128, 32 and 48
Length of all dipoles and quadrupole	2332.7 m
Total Length of MI	3319.4 m
Beam Pipe in the arcs minor/major radii	2.39 / 5.88 cm
Beam Pipe radius in straights	7.46 cm
Beam Pipe Material	16 gauge 316L stainless steel
Secondary Emission Yield 300 eV	$1.0 - 3.0$
Vacuum	$\approx 2.0\,10^{-8}$ Torr
Max. Num. of Protons per bunch	$1.0\,10^{11}$
Longitudinal emittance per bunch	$0.8 - 2.6$ eVs
Bunch Length	1 m to 0.3 m
Bunch Spacing	18.9 ns
Number of bunch per batch	70
Number of empty bunches between gaps	4
Abort gaps	$2 \times 0.8\mu$sec
Maximum number of batch	6
Number of bunches per batch	82
Empty bunches at end of batches	3
Normalized transverse emittance	15 to 25 π mm mRad
$\beta_x \sim \beta_y$ in the arcs	11 to 56 m
Bunch transverse size 20 GeV (r.m.s.)	≈ 3 to ≈ 6 mm
Beam Pipe Frequency Cutoff (in dipoles)	1.49 GHz
Microwave Frequency	1.538 GHz
Space between Emitter/Receiver	~ 13 m

Throughout this calculation, the MI is assumed to be at ≈ 20 GeV, close to transition, where the bunch length is shortest. This energy has been chosen because the EC effect is most pronounced when the electric fields created the proton bunch are most intense, that is, when the bunches are short. The transverse beam size quoted on table I are realistic as they are based on real measurements [18, 19][1]. This emittance is in part dictated by the performance of the Fermilab 8 GeV Booster and associated transfer beam lines, the resistive wall instability (mitigated by the use of a damper system [21]), and possibly by the EC effect.

As shown later, the EC is a localized phenomena, particularly in a strong confining magnetic field. Thus, the short sections can be used to study in detail some the dynamical aspects of the cloud with limited compute power. The long section allows us to study the EC for a variety of magnetic fields and is also used for the simulation of the microwave experiment.

The propagation of a bunch train is simulated for about a fraction of one microsecond. Such a short time with respect to the cycle time of the synchrotron or even the duration of one Fermilab Booster batch (1.6 μ sec) is justified because the EC quickly reaches saturation ($\sim$ 100 ns), if dense enough. If the EC is thin, or evanescent, then longer simulations are needed. However, such cases are of little interest as the ECs will not cause beam instabilities.

C. Our main simulation tool: VORPAL

VORPAL[6] is a fully 3D code and self-consistent. By this we mean that, within the precision dictated the cell size and the time step, the kinematics of the electrons is correctly dictated by the EM field configuration and all fields are taken into account. All such calculations are 3D without requirements on symmetries of the boundary condition. The Courant condition that sets the consistency of the time step regarding to the cell size is always satisfied.

The Furman & Pivi[22] model for secondary emission has been implemented in the Tx-Physics library [23], which is extensively used by the VORPAL code. In addition, the Vaughan model [24] has been implemented and an arbitrary SEY can be uploaded, allow-

[1] This is based on recent measurements using the ion profile monitor. Such measurement are a within 10 % of the advertised performance stated in reference [19]

ing us to quantitatively determine the sensitivity of the EC effect to the so-called "true secondary" emission yield.

VORPAL runs on leadership class machines, such as the Blue-Gene P or the Cray-XT. Parallelism is implemented in such a way that the casual user does not need to know nor understand the message passing interface MPI. However, targeted problem decompositions have been used to optimize performance, as discussed below. Most of the CPU intensive runs were done using the Intrepid Blue-Gene P at the Argonne Leadership facility, using approximately 9.5 million core hours.

1. *EC VORPAL scripts and running conditions.*

As any general purpose codes, VORPAL needs to be customized to the specific problem at hand. This is done by writing specific scripts, which define the physical configuration of the currents and boundaries, initial condition of the cloud and electron emitters. A summary of the salient parameters is given on table II

The cell size is dictated by the smallest feature in the problem, which, in our case is either the transverse beam size, or the physical size of the slits in the RFA's. Systematic uncertainties are estimated by simply looking at relative changes of the relevant quantities, such as the electron density of the EC, or the voltage on the simulated antenna in the case of the microwave absorption experiment, as a function of grid size. Those listed on table II are therefore typical and were not rigidly set at the onset of the calculations.

Two distinct types of boundaries are used: The elliptic (or cylindrical) beam pipe, transverse to the beam and the Perfectly Matched Layers (PML). These later types of boundaries emulate an infinitely long beam pipe on either end of the region of interest. They are particularly needed in detecting quasi plasma wave and the simulation of the microwave absorption experiment.

The initial state of the electron cloud, unless otherwise specified, is defined as follows. All electrons have negligible velocities, and are distributed uniformly along the beam axis, awaiting the passage of the first bunch. On the transverse plane we have a simple 2D Gaussian distribution, $\approx 3\times$ broader than the beam. Fortunately, the details of this initial state are inconsequential, as they are completely forgotten after the passage of a few bunches. The initial density is set typically set at $2.5\,10^{11} m^{-3}$ and the maximum of macro-electrons

per cell is initially set to 15. Results at saturation are found to be stable against an increase of such initial conditions.

The static magnetic field configurations (stated above) as well as the current sources are implemented via VORPAL functions and macros. There are two distinct types of current source in the problem: the proton beam itself and the current source responsible for the emission of the microwave generation, only used in the case of the simulation of the microwave absorption experiment [11].

The electromagnetic solver for cell close to the curved boundary (e.g., the beam pipe) uses the Dey-Mittra [25] cut cell method. A Boris integrator/propagator is used for the relativistic macro-electrons particle. These macro-particles are weighted: as their number grows exponentially at the beginning, the EC is culled and the weights are re-assigned. The probability for a macro-particle to disappear or to be re-weighted is flat across the 6D phase space occupied by the EC. At any given time, all weights for all macro-electrons are identical.

The decomposition (i.e., the mapping of computational grid cells to computer nodes) is regular and cells that are physically close to each others along the beam axis are preferably implemented on the same processors. This specific decomposition is advantageous because, in most cases, the transverse magnetic field is strong enough to confine the electrons close to the field lines, thereby limiting the transport of electrons along the beam axis. Thus, it make sense to sparsify the problem along the beam axis.

Finally, VORPAL generates multiple output files. Beside the usual log file, the state of the EC is given as a collection of 6D phase space coordinates, the EM fields value for each cell and the so-called VORPAL *History* files are extensively used throughout this simulation. These files contain user-specified quantities recorded at every time steps, such the EM potential between two points, the number of macro-electrons, allowing us to get a precise detailed picture of selected quantities throughout the simulation.

D. POSINST

The EC phenomena in the Fermilab MI has been simulated prior to this work [7] using the "2D+" electrostatic POSINST code. Since VORPAL is a newcomer, it makes sense to compare the results obtained with VORPAL to previous results, and attempt to understand

TABLE II. Relevant Simulation parameters.

Parameter	**Value**
Phyla Length	from 0.25 m to 16 m
Beam Pipe geometry	elliptical, or cylindrical, as real
Magnetic fields	See above
Number of Grid cells (small con fig.)	720 X 48 X 24
Number of Grid cells (large con fig.)	6144 X 48 X 48
PM Ls length	$\approx$ 1 to 3 m
Typical Time step	3.12 ps
Typical Num. of time steps	10^5
Typical Num. electrons/cell	20
Typical Num. of processors	32 to 512
Beam Pipe geometry	elliptical, or cylindrical, as real
Bunch Length	0.3 m
Microwave frequency	1.538 GHz
Microwave Electric Field	20 to 100 V/m
BPM dist. emitter/receiver	3.5 m

the differences. This benchmark must be at the same time relatively simple and yet relevant to this complex problem. This much needed exercise has been successfully completed. For instance, agreement within $\approx 10\%$ on the electric field values close to the beam in a specific non-trivial case has been reached. A list of suggested improvements to both codes, shared privately with the participants has been discussed with the developers. Note that the realization of the dependency of the steady-state EC density on the initial condition for the seed cloud, described in the next section, has been quantitatively discovered in the process of the running this benchmark. Detailed methods and results are described in Appendix A.

III. RESULTS

A. Growth rate, saturation and decay rate of the EC.

The EC density, based on a VORPAL calculation, for a few different SEYs is shown on figure 2. The SEY curve follows the Vaughan model[24]. The long section of the beam pipe comprising two dipoles and one quadrupole has been used. A proton bunch intensity of $7.\,10^{10}$ is assumed. Evidently, both the growth rate and the saturation value of the density depends on the assumed SEY. Cases where the initial EC has a very long growth time, or the seed EC diffuses away, have not been studied extensively, as they correspond to an nonexistent EC problem. This occurs for $SEY_{max} \leq 1.3$. This critical SEY_{max} value is consistent with POSINST.

For relatively large SEY_{max} ($\geq 2.$), the saturation is reached after just a few bunches. Low energy secondary electrons emitted from the wall are no longer accelerated efficiently by the proton beam as they are repulsed by the pre-existing electrons from the cloud. This screening effect is a result of the self-consistency of the PIC (Particle In Cell) simulation. No ad hoc processes have been added to reach, or tune, this saturation. Average over ≈ 1 bunch width, the linear density along the beam axis (i.e., integrated over the transverse dimension) of the EC is about $70 \pm 10\%$ of the linear charge density in the bunch.

In absence of beam, electrons drift back the walls of the beam pipe. The decay rate of the EC is dictated by the average velocity along the magnetic field line. Typical values for this decay time range from 30 to 100 ns. Deviation for a simple exponential are substantial, because this decay is not a stochastic process, but a causal change, where fast electrons disappear first.

B. Sensitivity to initial condition.

This non-trivial feature of the EC problem was unveiled while benchmarking VORPAL against POSINST, where, at the onset, the spatial distribution of seed electrons were quite different. Such seed electrons trapped inside the beam pipe can be produced by either ionization of the residual gas, or produced at the wall by beam losses. While the density for such electrons is typically at least 2 or 3 orders of magnitude smaller than the EC density reached at saturation, the spatial distribution of these seed electrons does influence the final

EC density at saturation, as well as the induced electric field produced by the EC, shown on figure 1.

Various distributions of the seed electrons have been considered, corresponding to labels on figure 1:

- *Diffuse.* Our default case, where a diffuse seed cloud centered is centered on the beam region with a transverse width three times the width of the beam itself. This is also a compromise between the other extreme cases.

- *Beam Focused.* The seed could is centered on the beam, with a transverse width equal to the transverse width of the bunch.

- *Beam Focused, HD.* Same as above, but with a seed density 10 time higher.

- *Wall Electrons.* Electrons floating very close to the top and bottom beam pipe walls, above the beam region, (2 mm away and about 2 mm thick). In this case, it is assumed that these seed electrons are created by high energy proton hitting the beam pipe and such electrons are soft enough not to drift too quickly in between proton bunches.

- *Wall Elec. Thin.* Same as above, but at at density 10 times less.

Regarding the value of the electric field, note that the density of the seed cloud matters less than the geometry of the seed cloud. Thus, no detailed studies on the EC's seed density have been pursued. Note also that the the change of this field on the spatial distribution of the seed cloud is much smaller that the field due to space charge, in the $\approx 3\sigma$. However, the EC density close to the wall can differ by a factor two on such initial conditions.

Although a bit paradoxical, this phenomena has been reproduced by both VORPAL and POSINST codes. A putative explanation could be based on the existence of long time scale in the transverse diffusion rate in the cloud. More specifically, for a dipole field of 0.234 T, an electron temperature of the $\approx$ 40 eV, a spatial scale of 1 cm, the Bohm diffusion time scale is $\approx 5\,\mu$sec, assuming a typical distance of one cm. So, once the EC develops, it's pattern is nearly frozen transverse to the beam, suggesting a dependency on the initial conditions of the cloud, as shown by detailed simulation.

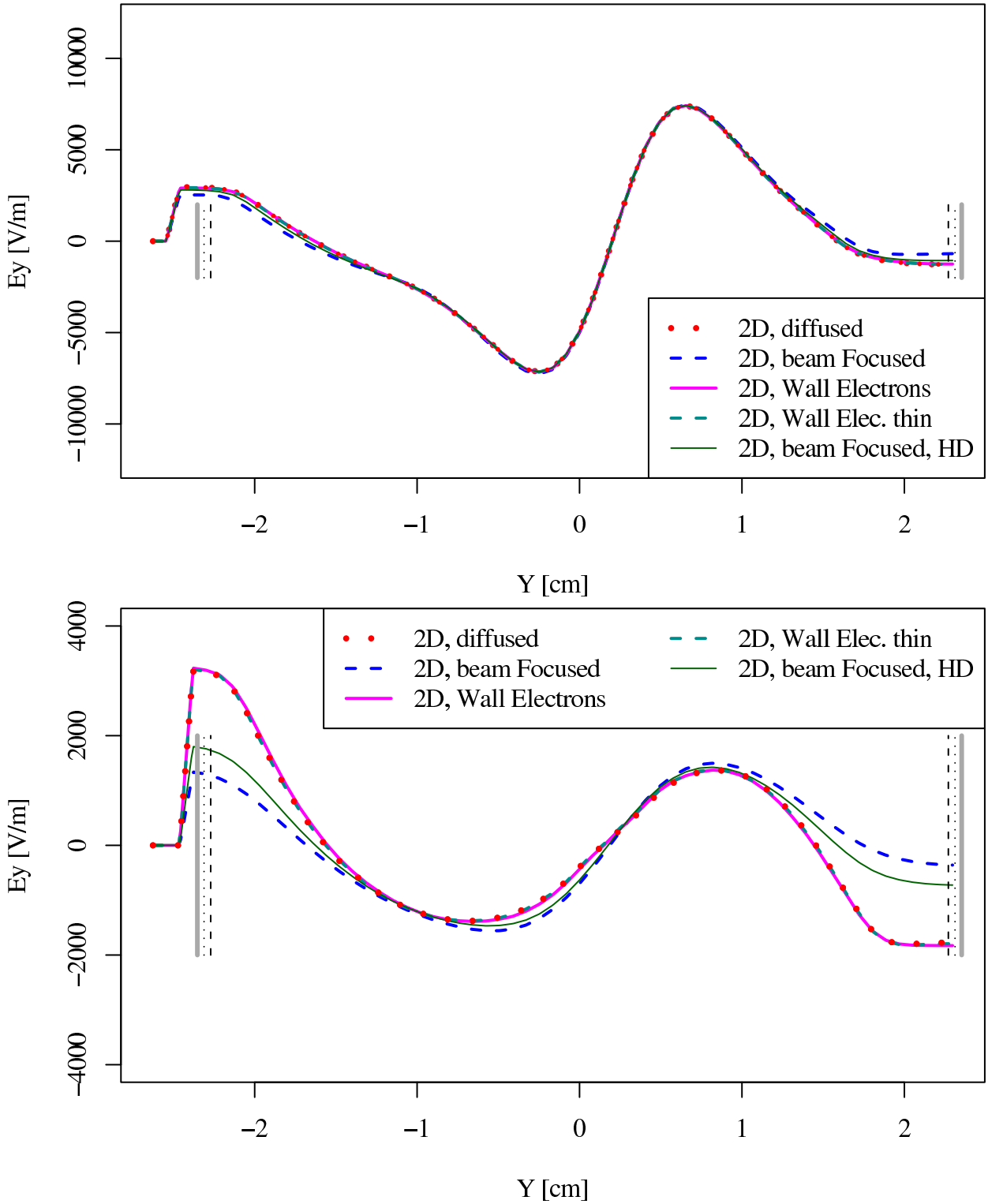

FIG. 1. The vertical electric field created by both the proton bunch and the EC at at t=524.085, for different initial conditions of the seed electrons. Top: at X=0. (symmetry axis) Bottom: same, but at X = 1.0 cm ($3.3\,\sigma$ away from the beam). The grey thick line indicate the location of the beam pipe walls and the dotted line the cell boundary that is closest to the wall. See text for details on initial conditions.

C. Sensitivity of the EC density to the SEY_{max} and the bunch intensity.

A critical issue for the Fermilab High Intensity frontier program[4] is to determine the additional beam disturbances and losses that are putatively caused by an enhanced EC problem. Unfortunately, given the uncertainty in the SEY_{max} for the "scrubbed" (i.e., processed by the beam) MI beam pipe, no reliable *ab-initio* predictions for the EC density and the related electric field maps can be generated at this point in time. However, if a moderate value for SEY is assumed - and this is justified by the fact that the EC problem does not currently limit the performance of the MI -, our result indicates that increasing the bunch intensity will not trigger a significant, non-linear, rise in the EC density, as shown on figure 3. This happens despite an increase of the peak electric field because the SEY no longer increases above ≈ 300 eV.

This happy conclusion seems robust against changes in the beam parameters: More intense bunches is likely to cause an increase the beam emittance (via space charge effects at injection, for instance), which itself implies weaker accelerating fields for the electrons in the cloud. Again, in this regime, the SEY weakly depends on the kinetic energy of the electrons.

D. Selected details on electron kinematics, Electric Field and plasma waves

Prior to discussING the experimental program, various observations on the morphology in 6D phase space of the EC are noteworthy. The spatial (longitudinal and transverse) distribution of the electrons in the cloud are shown on figure 4 and figure 5 and 6, respectively. The dynamics is also illustrated there via the rapid ($\approx$ ns) change in the local density of cloud. Except for about one ns just after the passage of the bunch, the highest density is always close to the wall and can be almost two orders of magnitude higher than at the center of the beam pipe.

The EC density depends on the confining magnetic field, even when the EC is nearly saturated. The fluctuations of the density during and in-between bunches has a non-trivial dependence on this magnetic field, as shown on figure 7 and 8 for large SEY_{max} and at stable saturation (i.e., the density averaged over one bunch crossing is stable over time). Also shown in this figure is the mean kinetic energy vs distance from the closest bunch.

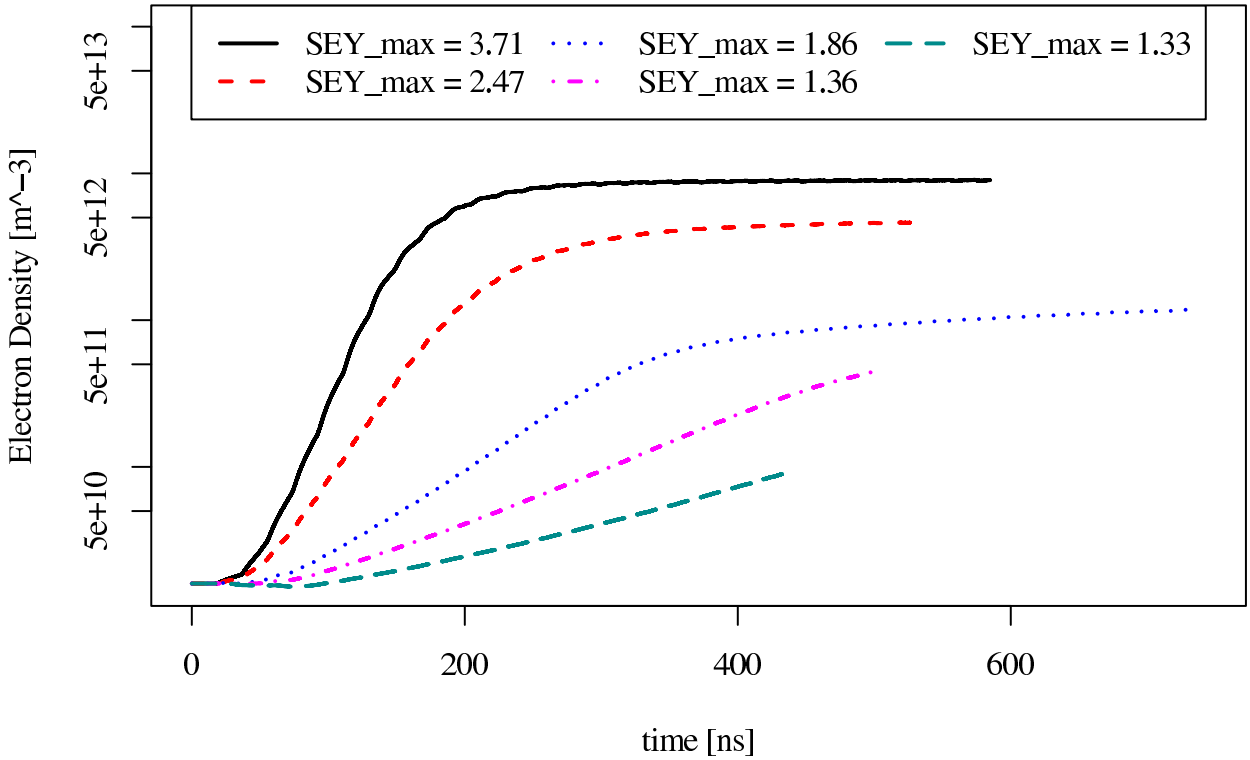

FIG. 2. The EC density vs time, at the beginning of a bunch train, for about 10 to 25 MI bunch spacing, illustrating the initial exponential growth and it's saturation, if the SEY is high enough. The seed density is arbitrary, but realistic. This illustrates the sensitivity to the maximum of the SEY.

Highest densities occurs in the drift regions, because net acceleration along the electric field lines induced by the passage of the proton bunch can occur in all transverse directions. The average kinetic energy is highest in the dipoles, presumably because the electric field created by the bunch, tends to be parallel to the magnetic field lines, allowing for efficient acceleration. Except in the fringe regions, the mean velocity along the beam axis is negligible compared the transverse velocities, even in absence of magnetic field.

For near critical SEY, the EC density vanishes in the quadrupoles and will be the highest in the field free regions, as shown on figure 9[2]

From these results, it is clear that the EC density fluctuates at 53 MHz (the bunch crossing frequency), with frequency components up to a few GHz (related to the bunch length.) It is also strongly anisotropic, with at least a strong quadrupole component, if not higher multipoles. Thus the EC will produce electromagnetic wave. While the low frequency

[2] By this, we mean the external $B_x = B_y = B_z = 0.$, within a small fraction of a Gauss.

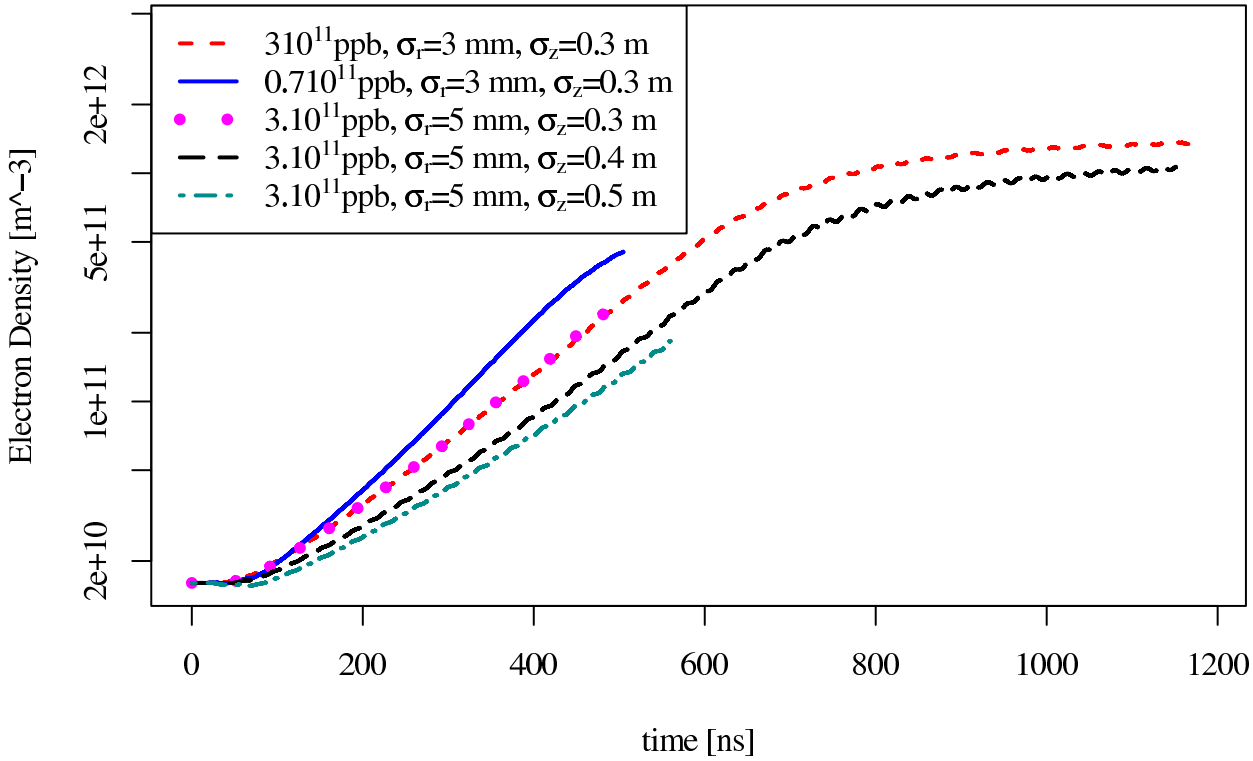

FIG. 3. Similarly to the previous plot, The EC density is shown vs time, for various beam conditions. σ_r and σ_z corresponds to the average beam radius and bunch length, respectively. These have been obtained assuming a moderate value of SEY of 1.36. If so, the worst case scenario corresponds to the current operating conditions and not those expected in the Project-X era.

component can not propagate in the beam pipe (the cutoff for the fundamental mode being at 1.56 GHz), higher order modes are induced and could be detected. In our simulation, the "pseudo-potential"[3] in between the top and bottom plates of BPMs is recorded for every time step. A straightforward Fourier transform reveals these electromagnetic waves produced by the EC, as shown on figure 10 and 11. Such modes are characterized by their cutoff frequencies, the values obtained for such frequencies have been independently checked with the CST Microwave Studio package [29]. Evidently, such calculations must be done with the fully electromagnetic code, i.e., 3D VORPAL, and not the quasi electrostatic 2D code.

As in any complete PIC EM code, VORPAL also provided EM field maps. Of particular interest is the electric field induced by both the proton beam and the EC, as our ultimate

[3] The line integral of the electric field along a specific (and easy to compute) and fixed path, i.e., in our case, along the vertical axis.

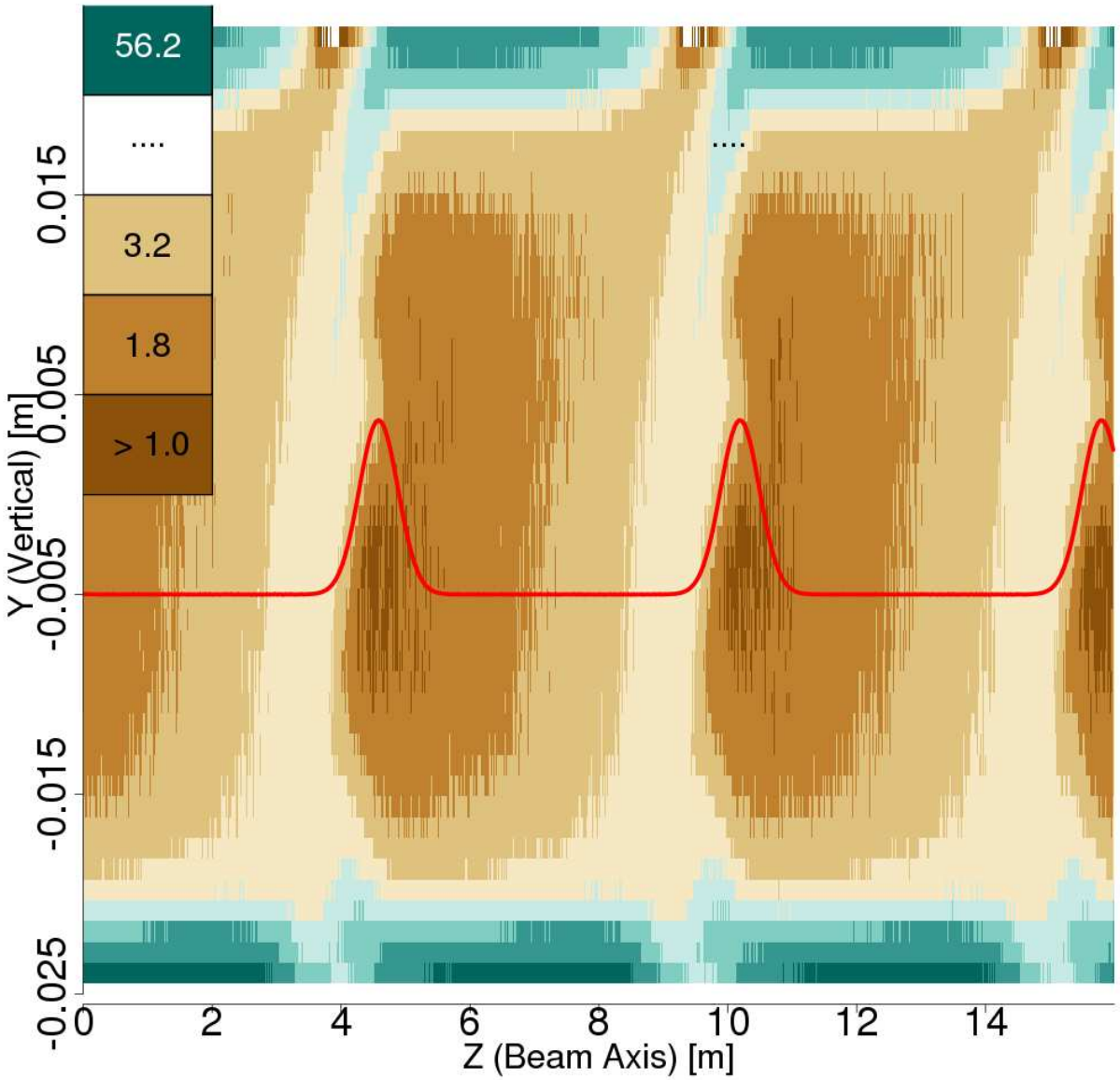

FIG. 4. An false color map of the longitudinal profile of the EC density in a dipole and for a continuous bunch train. The color scale is logarithmic. infinitely long dipole and a continuous sequence of bunches. The EC is fully saturated with $SEY_m \approx 2.2$. The proton bunch intensity is $0.7\,10^{11}$. The proton beam (red line) is displaced by 5 mm downwards, which makes the EC top-down asymmetric.

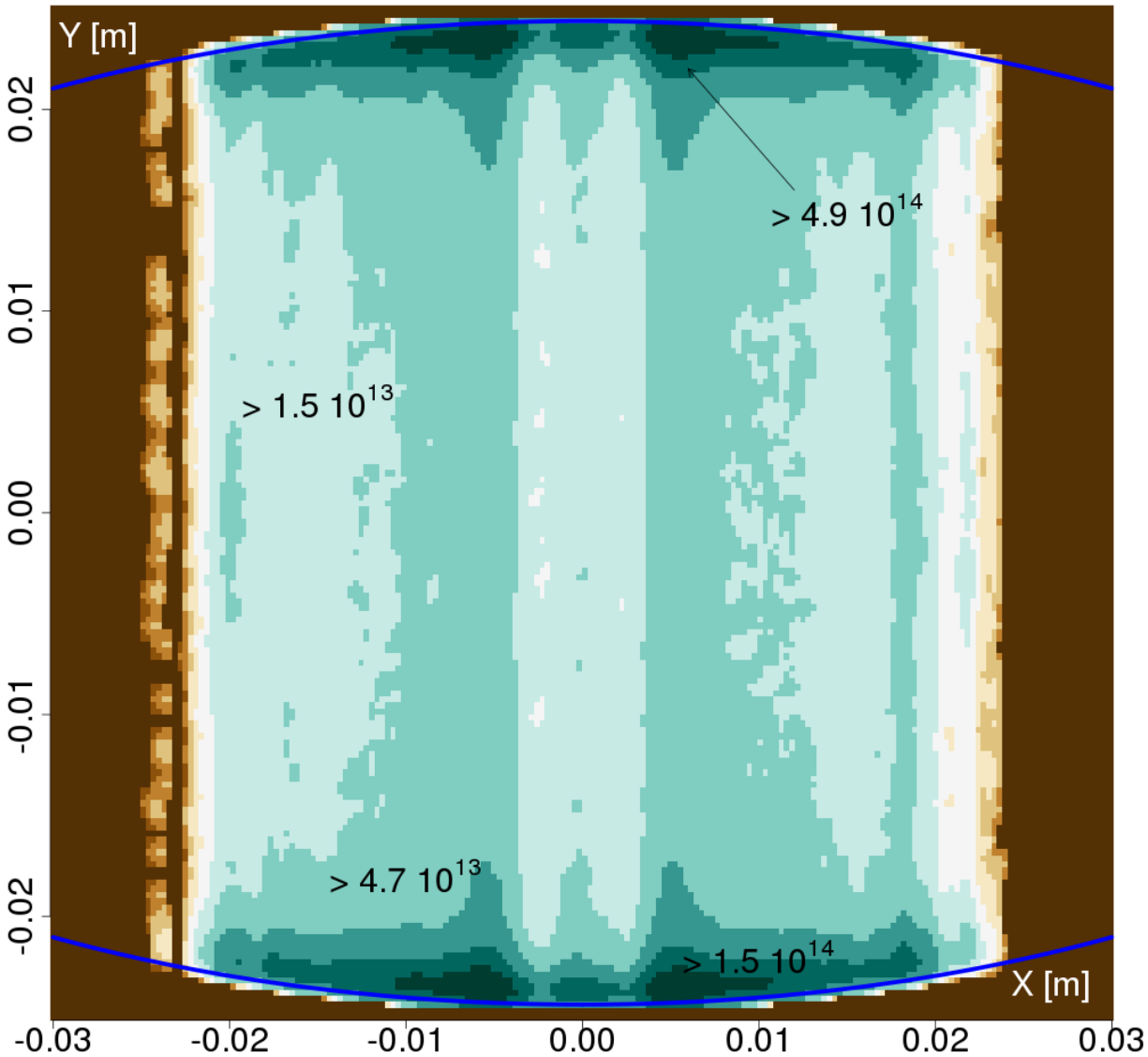

FIG. 5. Transverse profile of the EC density recorded at the beginning of the relaxation phase, when the density reaches a maximum.

goal is to model these fields such that they can be incorporated in advanced accelerator simulation codes that model non-linear and collective effects [30] Such an example field map is given on figure 12.

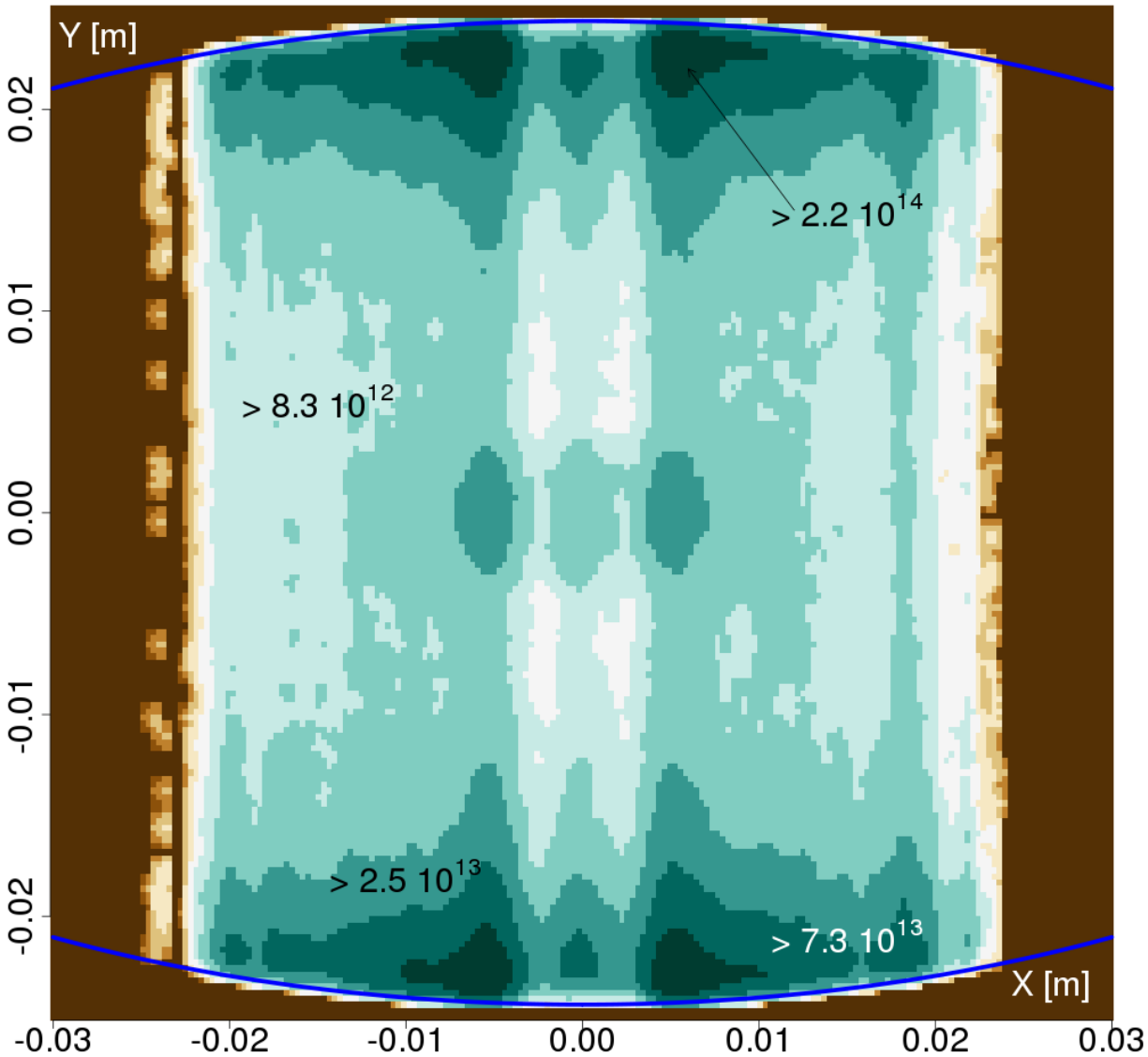

FIG. 6. Transverse profile of the EC density recorded during the pinch phase, when the density is minimum, as the electrons have just migrated away from walls and a diffuse excess is seen around the beam spot.

E. The RFA response

A few Retarding Field Analyzers (RFA) have been recently installed in a field free of the Main Injector, where the beam pipe is cylindrical, 6" diameter [10]. Slits allowing electrons to drift into these devices are located on top or bottom of the pipe and have transverse

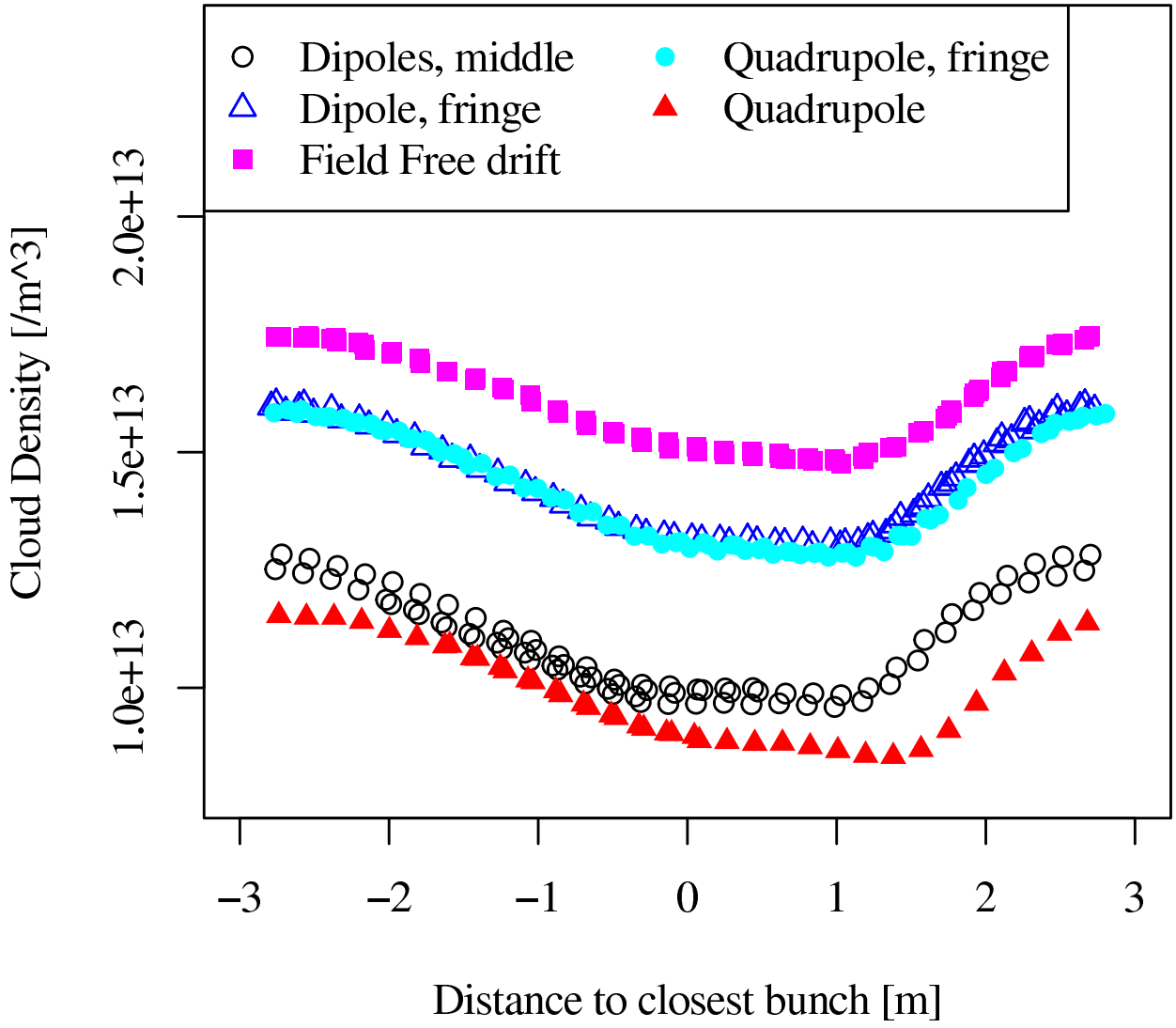

FIG. 7. Fluctuation of the EC density averaged over a 40 cm long section of the beam pipe as a function of the distance to the closest proton bunch, for different magnetic field configurations and a bunch charge of $0.7\,10^{11}$ protons

(longitudinal) openings of about 4 mm (2.5 cm), respectively. In VORPAL, such slits are simulated by simply setting the SEY to zero at their location. Fluctuations of the EC density at the slit location can then be extracted from the simulation and are expected to reflect the electron count in these RFAs. An energy cut can be applied to the VORPAL macro-electrons, thereby simulating the effect of the voltage applied on the RFA grid.

Abrupt variations of the electric field near the slits (Edge effects) are ignored in this crude model. A more exact implementation would include the precise geometry of the RFA grid

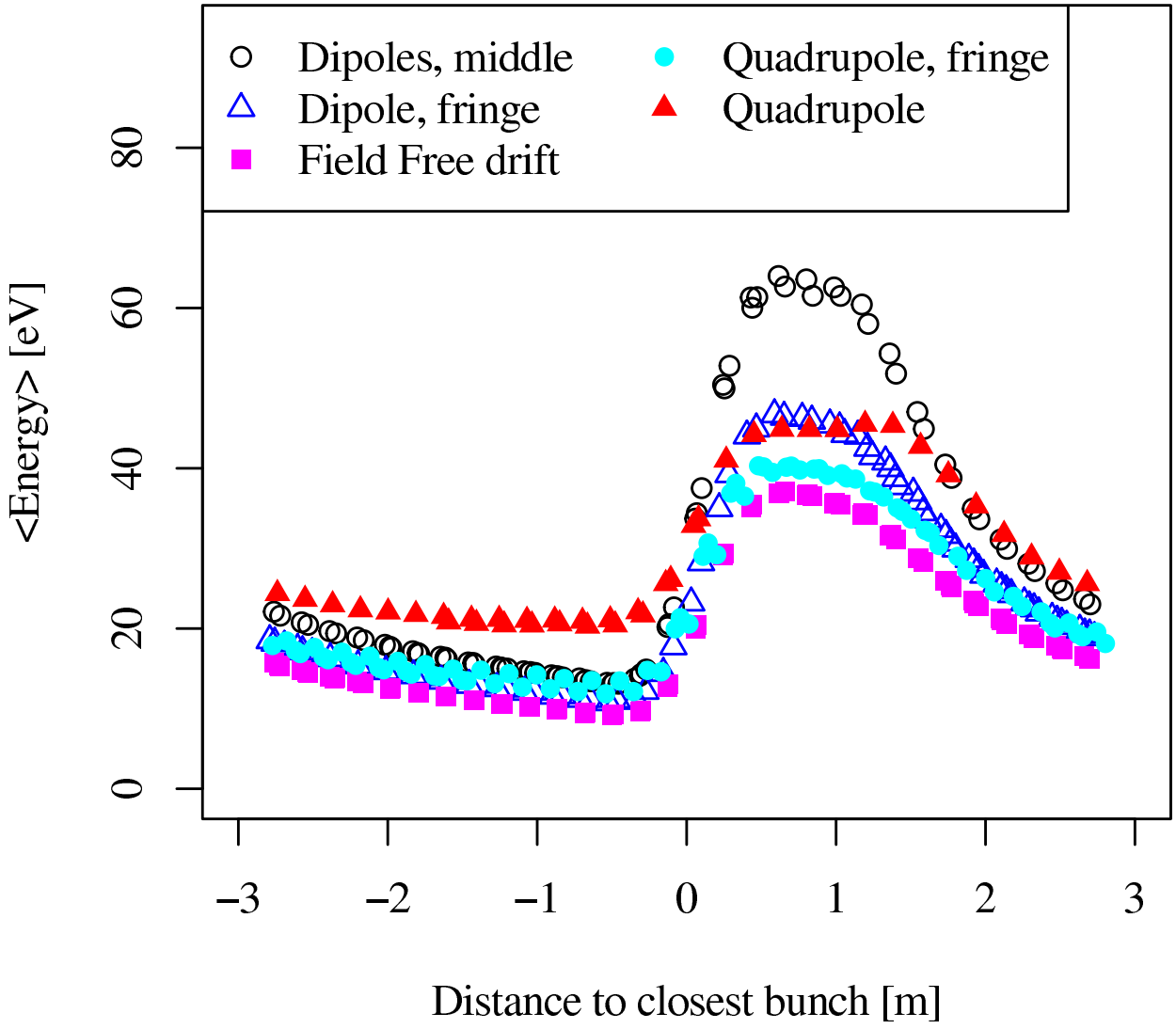

FIG. 8. The average kinetic energy of the electrons in the cloud for the same configuration as in the previous figure

and its detector. Since these detectors are quite small with respect to the total size of the beam pipe and VORPAL computational grid has to be uniform, this refinement has not been implemented. However, a much bigger uncertainty comes from the largely unknown stray magnetic fields due to the dipole and quadrupole bus that are running along the beam line. A field of $\approx$ 3 to 6 Gauss at one of the RFA location has been detected. More detailed maps will be required to compare data to simulation. Meanwhile, to illustrate the importance of weak magnetic fields in relation to the spatial distribution of the EC, figure 13 and 14 shows the transverse distributions of the electrons in the beam pipe for a uniform stray field of 10

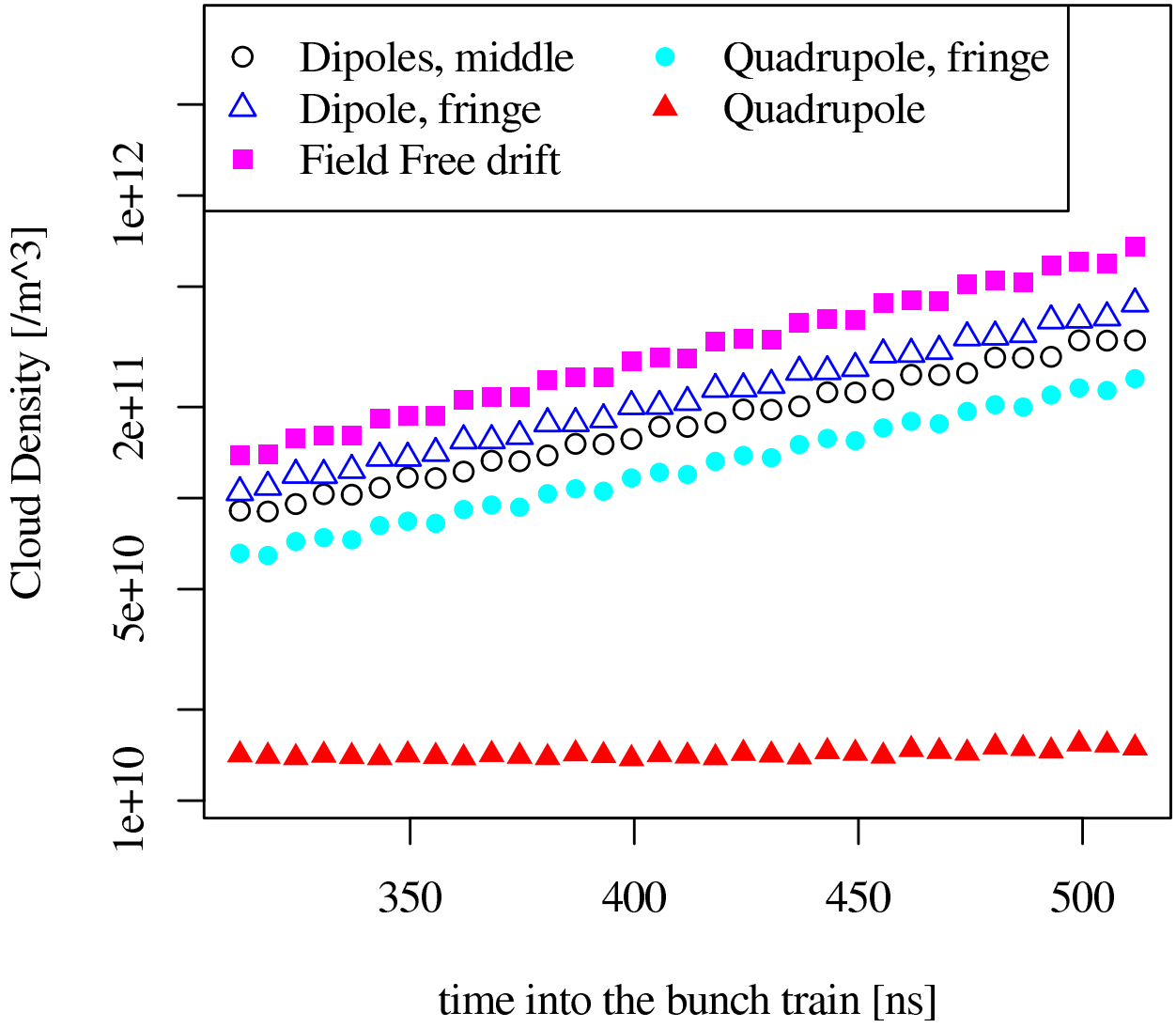

FIG. 9. Dependence of the EC exponential growth on the magnetic field configuration, in the case where the SEY is near critical.

Gauss oriented at 45 degrees, perpendicular to the beam axis.[4]

F. The Microwave absorption experiment

Multiple instruments are needed to characterize the EC. Microwave transmission measurements are non-invasive and relatively cheap to implement. The absorption and re-emission of microwave photons by the e-cloud causes a detectable phase shift in this microwave field.

[4] Magnetometers are being installed close to the RFA, allowing a more precise comparison of the data against simulation in the near future.

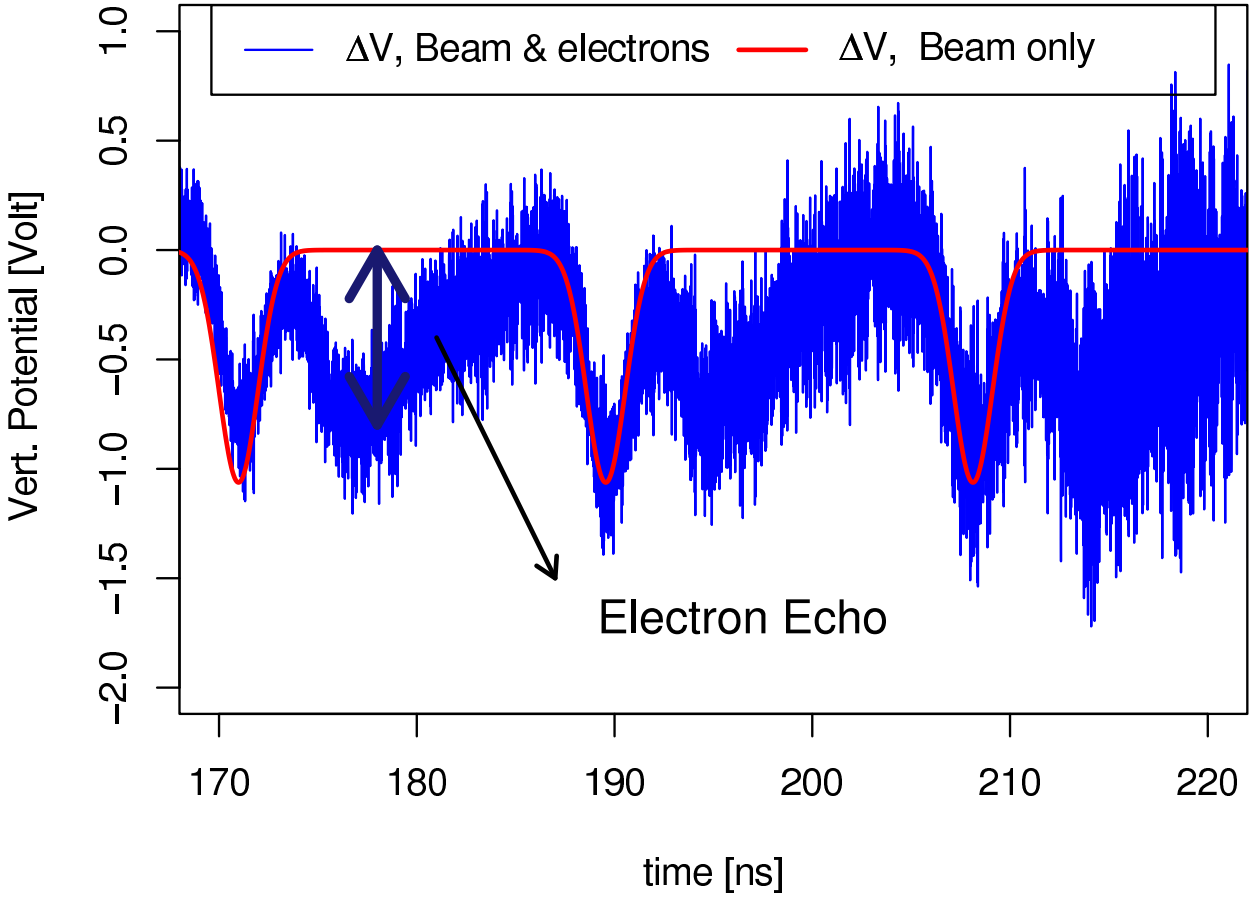

FIG. 10. The VORPAL pseudo voltage between the top and bottom plate of a virtual BPM in a dipole, when the beam is displaced vertically by 2.5 mm. In this case where the $SEY = 2.2$ and therefore the EC is saturated. About one ns after the passage of the bunch, the EC re-arrange itself, producing an "echo" signal.

This phase shift is related to the density of the e-cloud [31]. Our original intent was to compare our simulation results to real data taken at the MI [11]. However, significant problems were found at a later stage with the measurement technique: The chosen frequency was very close to the cutoff frequency of the elliptical beam pipe (≈ 1.54 GHz) and, consequently, the transmission efficiency was found to be depend critically on the details of beam pipe (pressure valves, bellows, etc) and to actually change during data taking. That is, the effective length between the receiving and emitting antennas was difficult to determine. Yet, for sake of completion, the phase shift calculated for the long (dipole, quadrupole, dipole) section of the MI is shown on figure 15. As in the simple linearized theory, the phase shift is a good measure of the density.

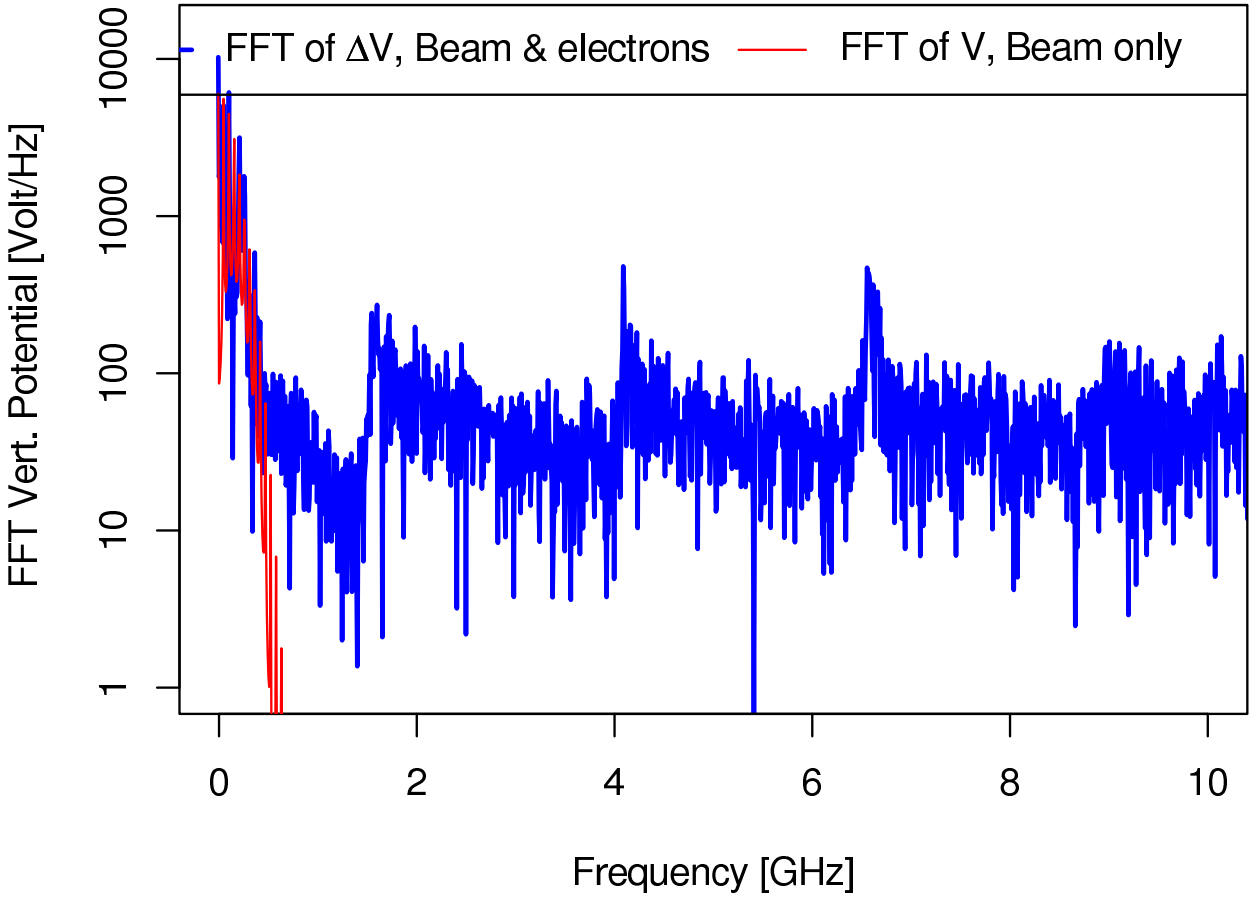

FIG. 11. The Fourier transform of the virtual BPM signal shown above, showing clearly the low frequency cutoff and the higher order mode for this elliptical cavity.

IV. SUMMARY

The electron cloud in the Fermilab Main Injector has been simulated in detail using a 3D and self-consistent code, VORPAL. This fully electromagnetic PIC code is relatively new to our EC community and has been bench marked against the existing POSINST code. Detailed and quantitive description of the dynamics of the EC have been explored. Existence of multi GHZ electromagnetic waves produced by the EC have been characterized. Electric field maps produced by VORPAL will be utilized for beam dynamics studies using codes such as Synergia [30].

While the uncertainty in the SEY and in the spatial distribution of seed electrons are such that no accurate predictions for the EC density can be made in the MI case, our results indicate that if the EC is thin enough not to cause beam instabilities under current beam

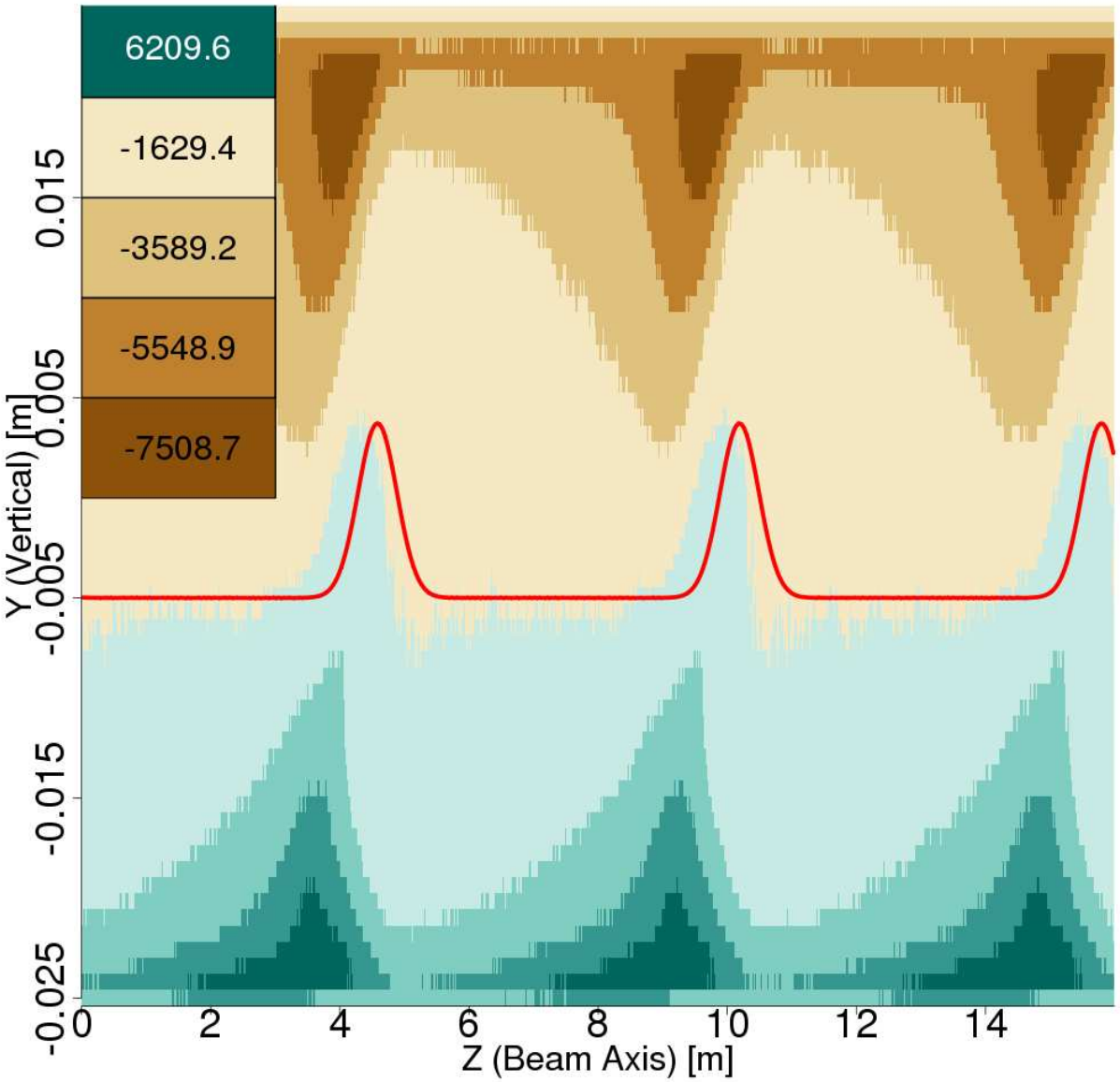

FIG. 12. A color map of the projected electric field produced by both the proton bunch and the EC. The setup and beam conditions are those corresponding to the results presented on figure 4.

conditions (bunch charge of $\approx 0.7\,10^{11}$), it is then likely that the SEY is rather low (≤ 1.36). In this case, our calculation shows that we should not see a dramatic (i.e, non-linear in the proton charge) increase of the EC density during the Project X era. In any event, further calculations using the Synergia [30] code on the impact of a dense EC on the MI beam will be pursued using the VORPAL field maps produced in the course of this study.

Despite the lack of precise predictions for the EC density, this simulation effort is worth-

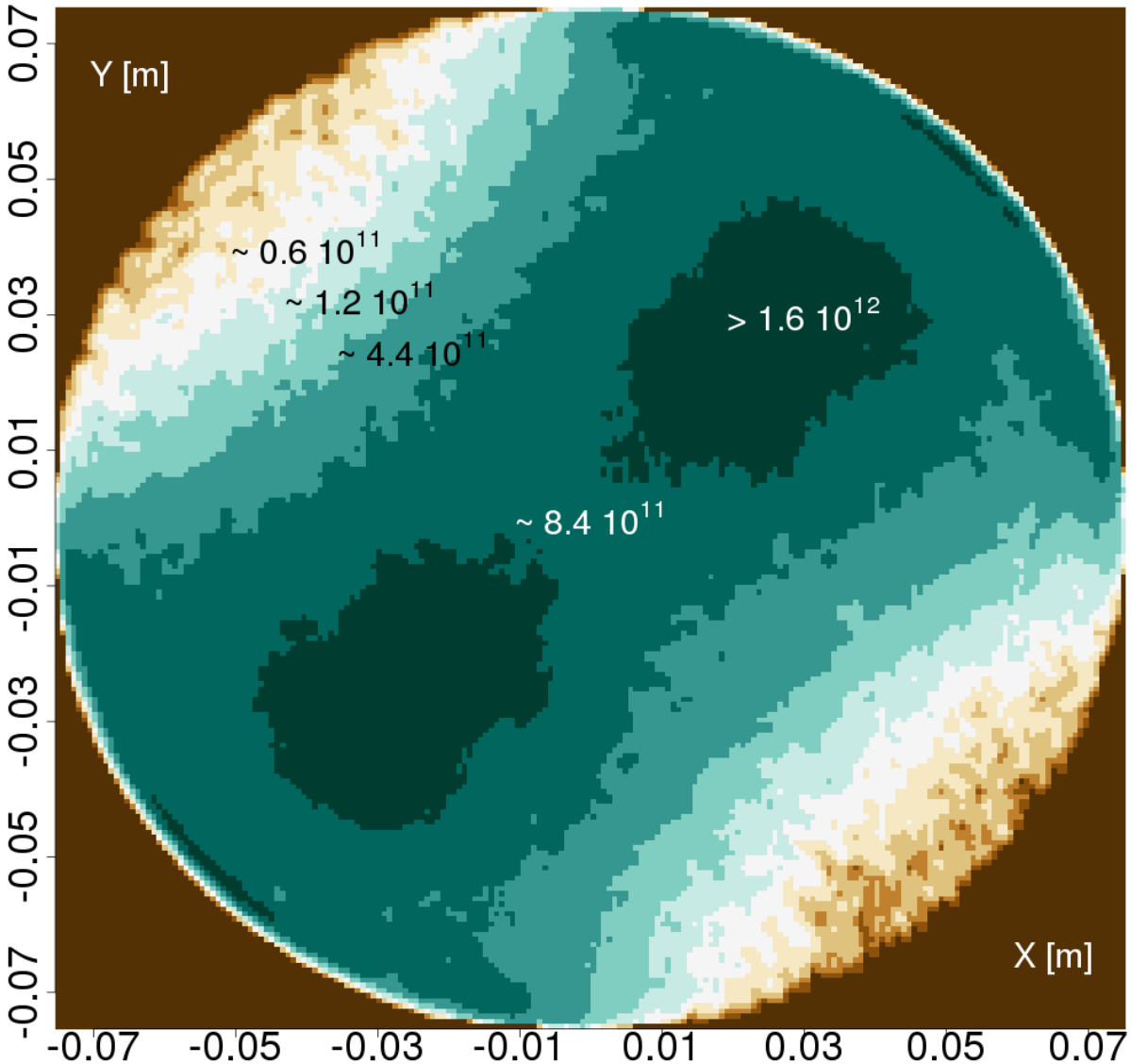

FIG. 13. A false color map of the EC density, transverse projection in the circular beam pipe supporting the RFA, as the EC is pinched by the passage of the bunch. The slits of the RFA are highlighted on the top of the cylindrical beam pipe.

while, as it provides guidance in establish a robust experimental program. More specifically, the value of the stray magnetic field at the RFA position must be determine. Since the SEY depends on the beam induced scrubbing, this crucial parameter must be determined *in-situ* and inside a magnetic field commensurate with the one used in the dipole or quadrupole. A dedicated set of two small dipoles equipped with instrumentation, retractable sample holder

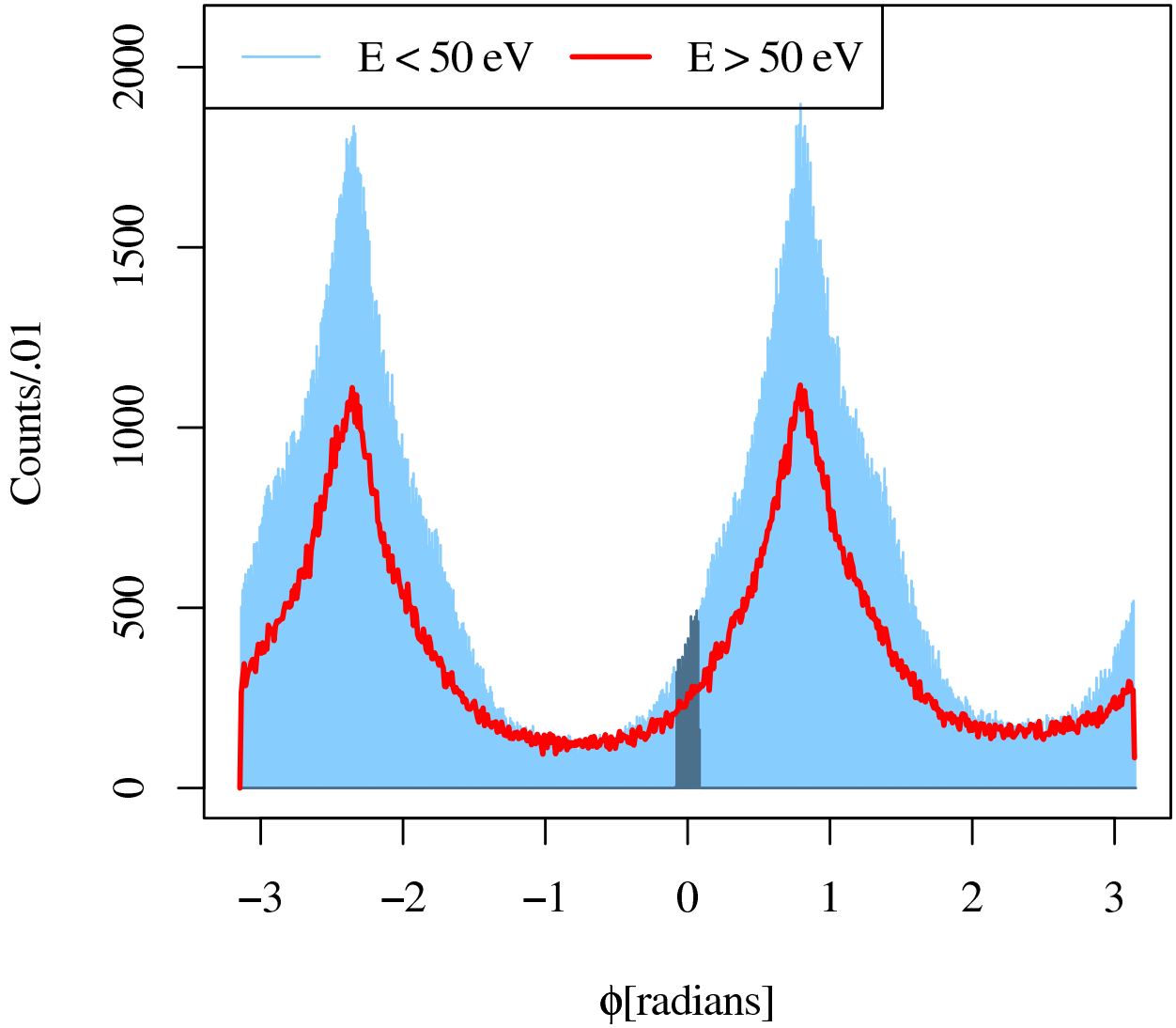

FIG. 14. A Histograms of the azimuthal angle from the simulated same data set. Again, the highlighted region is where the EC is sampled.

and an electron gun (to measure the SEY) should be installed in one of the available straight section of the MI.

A. Acknowledgments

We thank Jim Amundson and Bob Zwaska from the Fermilab APC group for very productive discussions on the analysis of the data generated by VORPAL. Xiaolong Zhang ran successfully the POSINST code for the benchmark. Manfred Wendt computed the eigen frequencies for the TE modes of the MI beam pipe, confirming the validity of Fourier spec-

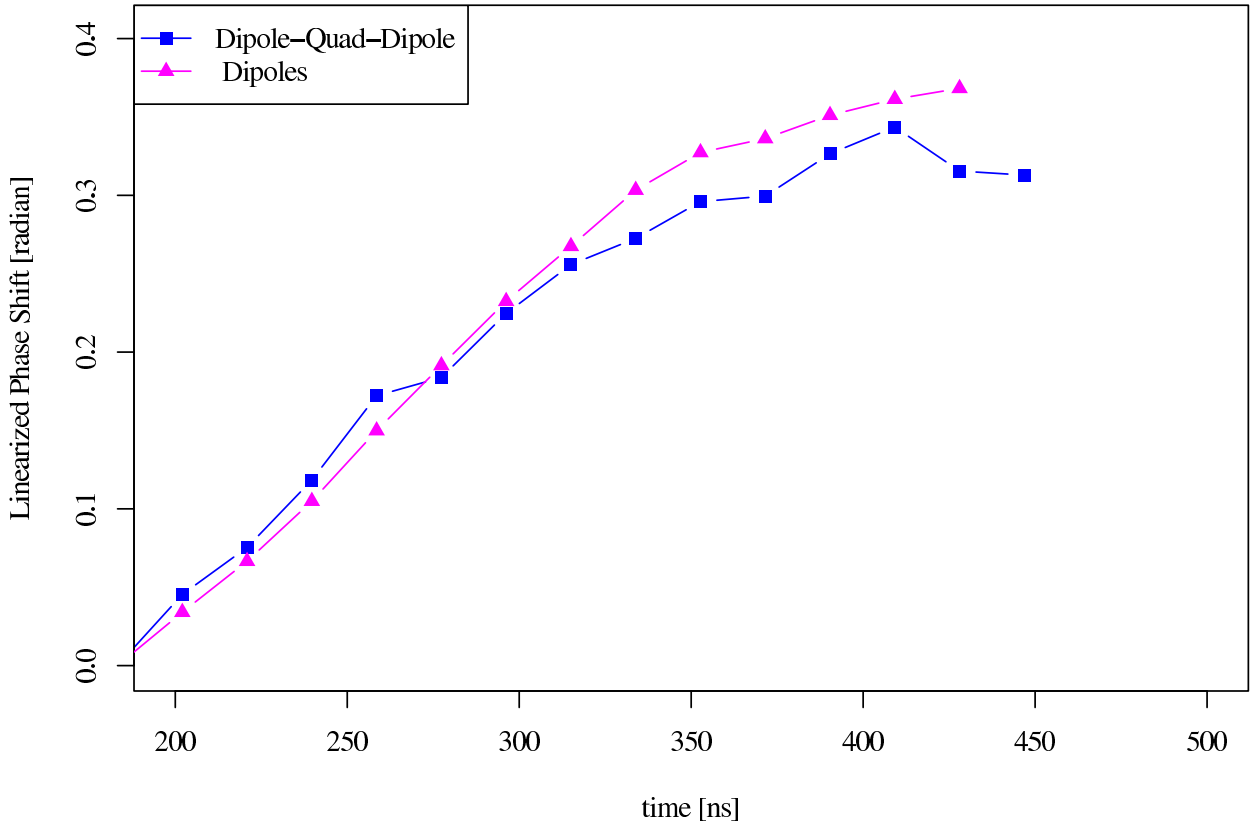

FIG. 15. The simulate phase shift for the infinitely long dipole and for a more realistic implementation of a short section of the MI. The setup and beam conditions are those corresponding to the results presented on figure 4.

tra shown in figure 11 We also acknowledge the other members of the VORPAL team: D. Alexander, K. Amyx, T. Austin, G. I. Bell, D. L. Bruhwiler, R. S. Busby, J. Carlsson, E. Cormier-Michel, Y. Choi, B. M. Cowan, D. A. Dimitrov, M. Durant, A. Hakim, B. Jamroz, D. P. Karipides, M. Koch, A. Likhanskii, M. C. Lin, J. Loverich, S. Mahalingam, P. Messmer, P. J. Mullowney, C. Nieter, K. Paul, I. Pogorelov, V. Ranjbar, C. Roark, B. T. Schwartz, S. W. Sides, D. N. Smithe, A. Sobol, D. J. Wade-Stein, G. R. Werner, N. Xiang, C. D. Zhou.

The check on the cutoff frequencies of the EC EM waves has been done by Manfred Wendt.

This work was supported by the United States Department of Energy under contract DE-AC02-07CH11359 and the ComPASS project funded through the Scientific Discovery through Advanced Computing program in the DOE Office of High Energy Physics. This research used resources of the National Energy Research Scientific Computing Center, which

is supported by the Office of Science of the U.S. Department of Energy under Contract No. DE-AC02-05CH11231. This research used resources of the Argonne Leadership Computing Facility at Argonne National Laboratory, which is supported by the Office of Science of the U.S. Department of Energy under contract DE-AC02-06CH11357.

Appendix A: Appendix: The POSINST-VORPAL benchmark

A realistic configuration of the beam pipe (elliptical see table I) and the static magnetic (0.234 T.) is implemented for both package. The same transverse grid size and the same SEY parameters are used. To avoid over-simplification, the beam is displaced vertically by 2.5 mm with respect to the center of the beam pipe. A relatively high SEY is used (reaching 2.2 at 300 eV) allowing us to shorten the growth time period and stress the codes as the final density is higher than for evanescent ECs. A difference between VORPAL and POSINST relates to the dimensionality: VORPAL can either run as a 2D or 3D code, while POSINST is strictly a "2D+" electrostatic code. In POSINST, the proton bunches are sliced longitudinally an only the transverse electric field is considered. Within a given slice, the acceleration due to the transverse space charge of the proton bunch is computed analytically while the contribution due to the transverse space charge from the EC is obtained via a numerical Poisson solver. While longitudinal acceleration are neglected, transport equations for the electrons in the static magnetic field are numerically solved in 3D space, for a given time slice. This 2D+ approximation is fully justified as long as the confining magnetic field is much larger than the transient magnetic field produced by the proton beam: net acceleration of the electrons occurs only along the field lines. Therefore a 2D, time dependent, "electrostatic" calculation is allowed, as long as EM waves generated by the EC are ignored. By this, we mean that all magnetic field are static and external, unrelated to the velocities of charged particles and that accelerated charges due to electric field do not radiate. These approximations have been tested in the VORPAL context and in the restricted case of a the strong dipole field, where the electron motion is confined along the magnetic field. The 4D proton beam current has been reduced to a time dependent charge density, neglecting the longitudinal current and thereby the magnetic field induced by the beam. The VORPAL number of spatial dimension is set to 2. Indeed, in this case, the EC density obtained in electrostatic VORPAL in this 2D case and the usual 3D case are consistent. Since this "2D+" problem is a lot simpler to

solve then the full 3D case, this benchmark is done using the 2D electrostatic VORPAL.

VORPAL is fully parallelized, while POSINST version 15, patch 3, used in this benchmark, runs on single CPU. However, for this benchmark at least, CPU time consumption was not found to be a problem.

As shown above, the density changes rapidly near the walls of the beam pipe. Consequently, one has to refine the grid near the curved surface to maintain accuracy. Integrated over the entire volume, changing the transverse grid size from 32×32 to 64×64 changes the estimate of the EC density by 20%. Fortunately, what counts is the EC density in the beam region: the EM forces on the protons induced by either free electrons very close to the beam pipe or on the beam surface are small, and nearly identical. Thus, we focused out attention on a 1 beam sigma cylinder centered on the beam. There, the a change of a factor 2^2 in grid size gives at most a 14% change in density. These are VORPAL results.

Since the seed EC are completely different in VORPAL vs POSINST, the onset of the exponential growth can not be compared. Therefore, the POSINST and VORPAL curves have been shifted along the horizontal axes, and only the growth rate (exponential in both codes) and the saturation value can be compared. On our first attempt, the EC densities in the beam region differed by a factor of ≈ 2. In addition, the growth rate was slower in POSINST [32]. The root-causes of these discrepancies have been thoroughly investigated.

The discrepancy was resolved by clarifying assumptions on inputs to the simulation and testing each part of the problem separately:

- The electric field produced by the proton bunch. In VORPAL, this $\vec{E}$ field is computed at every time step from the proton bunch charge density using a numerical Poisson solver. Such field maps can be downloaded at any time step for offline studies. In POSINST, this field can be derived from the set of "beam kicks": tables of $q\vec{E}/m$ values, where q is the electric charge of the electron, $\vec{E}$ and m the electron mass. These are computed at initialization time at all grid locations using analytical formulas valid for Gaussian beams. Despite the differences in methods, the $\vec{E}$ values do agree within a few percent, relative, from a σ away from the core of the beam or a few mm away from the beam pipe wall.

- The next set of initial conditions to be considered is the 6D phase space distributions of primary (or "seed") electrons prior to the exponential growth due to beam/wall

multipacting phenomena. In POSINST, such seed electrons are continuously generated, while in VORPAL, a static seed EC was declared at the onset. As documented in section III B, the spatial distribution of these seed electrons does matter, and were found to disagree significantly for both packages. This was found to be the most relevance difference. This dependency on initial conditions was explored in each package separately. Moreover, the POSINST has a convenient utility that allows the user to upload an arbitrary phase space simulation for the EC, and restart the simulation process. A VORPAL, saturated and steady state , obtained after ≈ 25 bunch crossing has been uploaded in POSINST, thereby rendering the differences in the initial condition a moot point. This brings the two code in acceptable agreement.

- The secondary production model has also been studied carefully, in particular the multiplicity of electrons produced at the beam pipe wall. Here, by construction, the physical assumptions and the modeling do agree, as VORPAL uses the TxPhysics library, which is based on the same Furman-Pivi [22] model used in POSINST code. However, an optimization was introduced in POSINST in generating the probabilities to produce a given number of electrons, causing a slight difference at high secondary emission yield and high electron multiplicity. Once that was understood, the steady-state VORPAL EC uploaded in the POSINST remains is preserved, bunch to bunch, within the expected accuracy, when being handled by POSINST.

- To avoid incidental agreement between the two packages, where two distinct errors would cancel out, further tests were devised. For instance, the electric field produced by the EC just after the upload in POSINST were compared in absence of beam/wall multipacting, by turning off the secondary emission yield in both packages. The time dependence of the field is a non-trivial function of the Poisson-solved field itself, checked just after the upload of the steady state EC, and the propagation of the electrons in the combined EM fields, which were checked out separately prior to this test. The comparison of the POSINST vs VORPAL is shown on figure 16, 5 mm away from the wall, or about 7σ away from the proton beam. The agreement does improve as one moves away from the wall.

This type of benchmark exposes the numerical uncertainties quite effectively. For instance, should the knowledge of the electric field close to the wall with a relative accuracy of

≈ 10% be really needed, a further drastic increase in grid resolution will be required. This is certainly affordable in VORPAL 2D on leadership class machine as it is parallelized quite effectively, but a bit more tedious with POSINST, as this application runs on single cores.

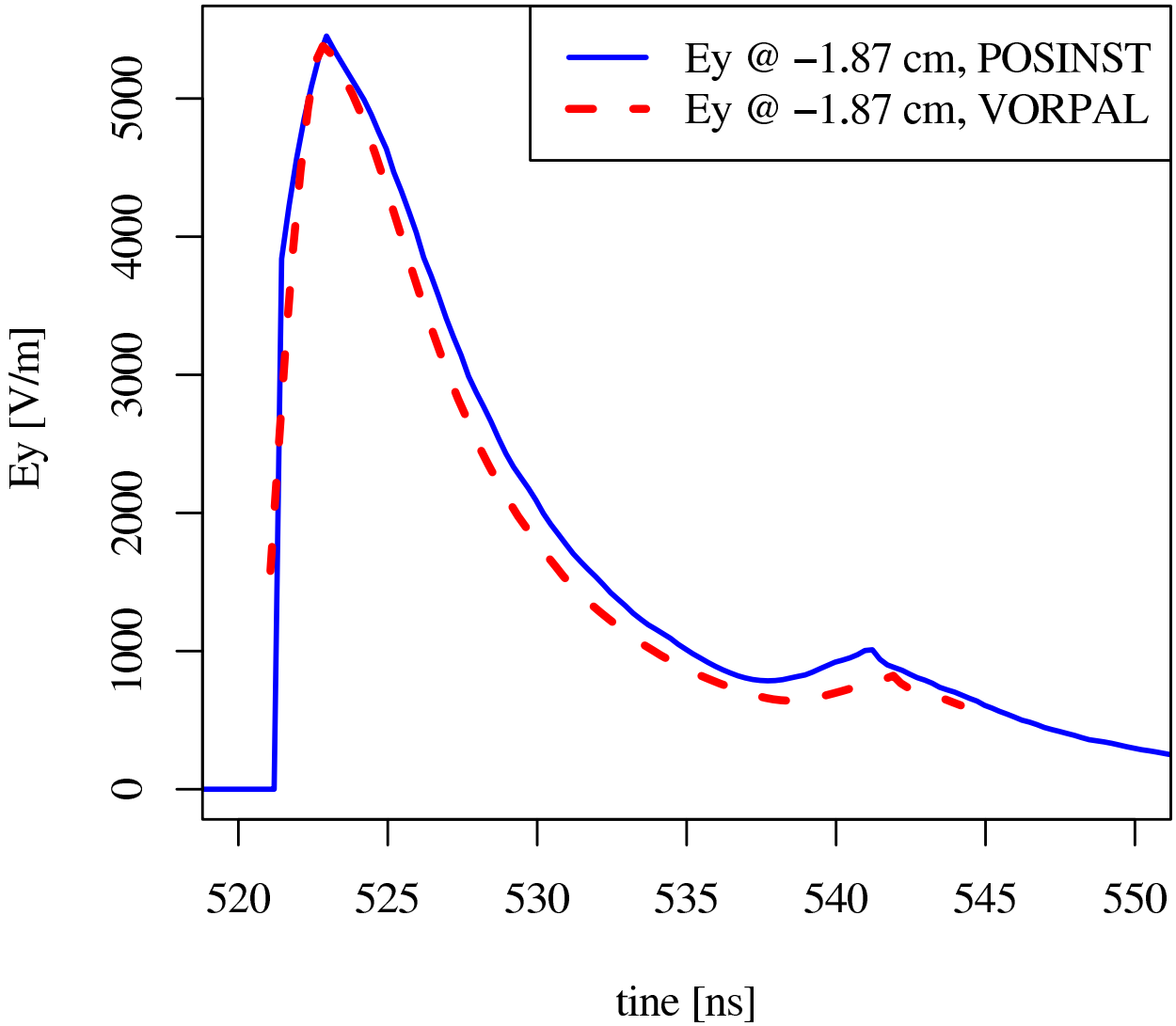

FIG. 16. The vertical electric field produced by the steady state EC, at $x = 0$. All production of secondary electrons is turned off at the time of the upload in POSINST ($t = 521.1$ ns). The density decreases as electron drift to the wall. Consequently, the field produced by the EC also decreases. The perturbation due the next bunch is seen at $t \approx 539.8$ ns.

[1] F. Zimmermann, Phys. Rev. ST Accel. Beams **7** (2004).

[2] M. T. Pivi and M. A. Furman, Phys. Rev. ST Accel. Beams **6** (2003).

[3] M. P. *et al.*, "Electron cloud at low emittance in cesrta," http://accelconf.web.cern.ch/AccelConf/IPAC10/papers/tuymh02.pdf (2010).

[4] S. Holmes, "Project x: A multi-mw proton source at fermilab," http://accelconf.web.cern.ch/AccelConf/IPAC10/talks/tuyra01_talk.pdf (2010).

[5] *et al.*. C. Yim Vallgren, "Low secondary electron yield carbon coatings for electron cloud mitigation in modern particle accelerators," http://accelconf.web.cern.ch/AccelConf/IPAC10/papers/weoamh03.pdf (2019).

[6] C. Nieter and J. R. Cary, J. Comp. Phys. **196** (2004).

[7] X. Z. *et al*, "Electron cloud studies at tevatron and main injector," http://accelconf.web.cern.ch/AccelConf/p07/PAPERS/THPAN117.PDF (2007).

[8] A. G. *et al.*, in *Proceedings of the 31st ICFA Beam Dynamics Workshop:Electron Cloud Effects*, Napa, CA, edited by M. Furman (2004).

[9] Evidently, this is not true over long distances and many turns. However, our simulation produces field maps that can be incorporate into the Synergia framework where numerous collective effect can be studied. This will allow us to study the impact of the EC on the beam itself.

[10] R. Z. C.Y. Tan, K.L. Duel, "An improved retarding field analyzer for electroncloud studies," http://accelconf.web.cern.ch/AccelConf/PAC2009/papers/th5rfp041.pdf (2009).

[11] N. E. *et al*, "Measurement of electron cloud development in the fermilab main injector using microwave transmission," http://accelconf.web.cern.ch/AccelConf/PAC2009/papers/we4grc02.pdf (2009).

[12] S. D. Holmes, "The fermilab main injector technical design handbook," http://www-fmi.fnal.gov/fmiinternal/MI_Technical_Design/index.html.

[13] T. Asher and S. Baginski, "The main injector rookie book," http://www-bdnew.fnal.gov/operations/rookie_books/Main_Injector_v1.1.pdf.

[14] B. H. *et al.*, "The variation of the secondary electron yield and of the desorption yield of copper under electron bombardment: origin and impact on the conditioning of the lhc," http://cern.ch/AccelConf/e02/PAPERS/WEPDO014.pdf (2002).

[15] N. H. *et al.*, "The secondary electron yield of technical materials and its variation with surface treatments," http://cern.ch/AccelConf/e00/PAPERS/THXF102.pdf (2000).

[16] J. R. Z. *et al*, "Fermilab main ring ion profile monitor system," http://cern.ch/AccelConf/pac97/papers/pdf/5P052.PDF (1997).

[17] F. Sauli, *Principles of Operation of Multiwire Proportional and Drift Chambers*, Tech. Rep. (1977).

[18] I. Kourbanis and D. Capista, Private communication (2010).

[19] S. D. Holmes, "Status of the fermilab main injector and recycler," http://cern.ch/AccelConf/pac97/papers/pdf/2B001.PDF (1997).

[20] This is based on recent measurements using the ion profile monitor. Such measurement are a within 10 % of the advertised performance stated in reference [19].

[21] P. A. *et al*, http://cern.ch/AccelConf/p05/PAPERS/MPPP015.PDF (2005).

[22] M. A. Furman and M. T. Pivi, Phys. Rev. ST Accel. Beams **5** (2002).

[23] H. S. *et al*, Phys. Rev. ST Accel. Beams **6** (2003).

[24] A. Shih and C. Hor, IEEE Transactions on Electron Devices **40** (1993).

[25] "Vorpal reference manual v4.2," http://www.txcorp.com/products/VORPAL/user_documentation/VorpalReferenceManual.pdf.

[26] Assuming a typical distance of one cm.

[27] By this, we mean the external $B_x = B_y = B_z = 0.$, within a small fraction of a Gauss.

[28] The line integral of the electric field along a specific (and easy to compute) and fixed path, i.e., in our case, along the vertical axis.

[29] http://www.cst.com/content/products/mws/overview.aspx.

[30] J. A. *et al*, "Simulation studies of the interplay between space-charge and impedance effects of the fermilab main injector," http://accelconf.web.cern.ch/AccelConf/HB2008/papers/wga08.pdf (2008).

[31] K. S. *et al*, "Simulation and analysis of microwave transmission through an electron cloud, a comparison and results," http://accelconf.web.cern.ch/AccelConf/p07/PAPERS/THPAS008.PDF (2007).

[32] P. L. G. L. *et al*, "Simulation of the electron cloud in the fermilab main injector using vorpal," http://edms.classe.cornell.edu/agenda/getFile.py/access?contribId=10\&sessionId=6\&resId=1&materialId=slides\&confId=10 (2010).